A constitutive framework for the non-Newtonian pressure tensor of a simple fluid under planar flows

Remco Hartkamp,[1,a)] B. D. Todd,[2,b)] and Stefan Luding[1,c)]
[1]*Multi Scale Mechanics, Faculty of Engineering Technology, MESA+ Institute for Nanotechnology, University of Twente, P.O. Box 217, 7500 AE Enschede, The Netherlands*
[2]*Mathematics Discipline, Faculty of Engineering and Industrial Sciences and Centre for Molecular Simulation, Swinburne University of Technology, Hawthorn, Victoria 3122, Australia*

(Received 13 February 2013; accepted 28 May 2013; published online 27 June 2013)

Non-equilibrium molecular dynamics simulations of an atomic fluid under shear flow, planar elongational flow, and a combination of shear and elongational flow are unified consistently with a tensorial model over a wide range of strain rates. A model is presented that predicts the pressure tensor for a non-Newtonian bulk fluid under a homogeneous planar flow field. The model provides a quantitative description of the strain-thinning viscosity, pressure dilatancy, deviatoric viscoelastic lagging, and out-of-flow-plane pressure anisotropy. The non-equilibrium pressure tensor is completely described through these four quantities and can be calculated as a function of the equilibrium material constants and the velocity gradient. This constitutive framework in terms of invariants of the pressure tensor departs from the conventional description that deals with an orientation-dependent description of shear stresses and normal stresses. The present model makes it possible to predict the full pressure tensor for a simple fluid under various types of flows without having to produce these flow types explicitly in a simulation or experiment. © *2013 AIP Publishing LLC*. [http://dx.doi.org/10.1063/1.4810746]

I. INTRODUCTION

There is significant scientific and industrial interest in describing the relation between the pressure tensor for non-Newtonian fluids out of thermodynamic equilibrium and other quantities, such as the strain rate and the fluid density and temperature. Such relations would find applications for example in petrochemical and biomedical processes or in the flow of polymer melts. The behavior of simple monoatomic fluids is not nearly as complex as that for macromolecular fluids and colloidal system. Yet, even for simple fluids, no relation is known that accurately predicts the non-equilibrium pressure tensor for any arbitrary velocity field. Numerous computer simulations and experimental studies have provided insights into the behavior of sheared liquids and the normal stresses in an isotropically compressed liquid, while many other types of flows are far more difficult to create in a laboratory or with molecular dynamics simulations. If we are able to predict the non-equilibrium pressure tensor for any velocity field, it would reduce the experimental and computational efforts needed to design and improve fluidic devices. We introduce a framework in which the pressure tensor can be related to the flow (strain rate tensor) through carefully chosen invariants of the pressure tensor as a function of the velocity field. This framework is applied to a range of planar flow types with different field strengths.

Planar Couette flow (PCF), or (simple) shear, is by far the most studied and well-understood type of flow. It is perhaps the simplest type of flow to study via experiments (e.g., lubrication) as well as with non-equilibrium molecular dynamics (NEMD). Elongational flows are vorticity-free flows that contain contraction, stretching, or a combination of both. Such flows occur in several biological and industrial processes (for example, extrusion and moulding processes), but are generally rather difficult to study with NEMD simulations or experiments, since the dimensions of the fluid sample or simulation cell change with time, not allowing continuous deformation. Special techniques are needed to allow for simulations or experiments that can continue indefinitely, which is much easier in the case of shear flow. In planar elongational flow (PEF), a fluid element is compressed in one direction and stretched in another (perpendicular) direction, while the fluid element is not deformed in the third direction. If the rates of contraction and stretching are equal, also called pure shear, the flow is isochoric (i.e., the volume of the fluid element is a constant of the motion). In NEMD simulations of a bulk fluid, the primitive cell is surrounded by periodic images and the deformation of the cell follows the streaming motion of the fluid. The minimum allowable cell size in each direction is given by twice the cutoff distance of the interaction potential. If the cell size becomes too small, particles can interact with their own periodic image, which leads to non-physical results. Hence, the maximum simulation time would be limited by the cell size in the direction of contraction. This limitation on the simulation time can be avoided if reproducible boundary conditions can be found that are periodic in space and time. These boundary conditions remap the cell after each time interval τ_p, such that the simulation time is not limited by the deformation, and sufficient statistics can be accumulated. Kraynik and Reinelt[1] introduced such periodic boundary conditions for PEF, based

a)Electronic mail: hartkamp@mit.edu
b)Electronic mail: btodd@swin.edu.au
c)Electronic mail: s.luding@utwente.nl

on lattice theory. Todd and Daivis[2] later applied this method to NEMD simulations to perform various planar shear-free flows with longer simulation times than those that were previously accessible.

In the past, predominantly shear flow[3–6] and elongational flows[1,2,5,7–9] have been simulated due to their relative simplicity. Evans and Heyes[8] were the first to perform NEMD simulations of a fluid under combined elongation and shear, i.e., mixed flow. They were however limited by the lack of reproducible periodic boundary conditions valid for planar mixed flow (PMF) and not all simulations arrived at a steady state before reaching their maximum simulation time. Recently, Hunt *et al.*[10] developed suitable boundary conditions for PMF, based on the approach of Kraynik and Reinelt.[1] These periodic boundary conditions make it possible to study a wide range of flows that were previously not feasible to study with molecular dynamics. Hunt *et al.*,[10] and later Hartkamp *et al.*,[11] performed mixed flow molecular dynamics simulations in which the velocity gradient is a linear combination of those for shear and planar elongational flow

$$\nabla \mathbf{u} = \begin{bmatrix} \dot{\epsilon} & 0 & 0 \\ \dot{\gamma} & -\dot{\epsilon} & 0 \\ 0 & 0 & 0 \end{bmatrix}, \tag{1}$$

where $\dot{\gamma} = \partial u_x/\partial y$ is the shear rate and $\dot{\epsilon}$ the rate of elongation (stretching if component $(\nabla \mathbf{u})_{\alpha\alpha} > 0$, and contraction if $(\nabla \mathbf{u})_{\alpha\alpha} < 0$, where $\alpha = x$, y, or z). When the shear rate is zero, $\dot{\gamma} = 0$ and $\dot{\epsilon} \neq 0$, the flow simplifies to planar elongational flow and when the elongational rate is zero, $\dot{\epsilon} = 0$ and $\dot{\gamma} \neq 0$, the fluid is under shear flow. Shear flow and mixed flow have a non-zero vorticity that is proportional to the shear present in the flow $\omega = \dot{\gamma}/2$.

The velocity gradient can be homogeneously coupled to an atomic fluid via the SLLOD equations of motion:[12–15]

$$\dot{\mathbf{r}}_i = \frac{\mathbf{p}_i}{m_i} + \mathbf{r}_i \cdot \nabla \mathbf{u}, \tag{2}$$

$$\dot{\mathbf{p}}_i = \mathbf{F}_i - \mathbf{p}_i \cdot \nabla \mathbf{u} - \zeta \mathbf{p}_i. \tag{3}$$

A variant of this set of equations (the so-called DOLLS algorithm) was initially only developed for shear flow and uniaxial compression.[16] Later the SLLOD equations of motion (Eq. (3) above) were shown to correctly obtain the normal stress differences[3] and proven to be valid for arbitrary homogeneous flow.[14,15] The difference in the normal stress differences between the DOLLS and SLLOD formalisms for planar shear flow has also been shown in a computational study.[17] However, the authors did not account for the effect of the thermostat on the normal stress differences. Equation (2) represents the evolution of the position $\mathbf{r}_i$ of particle i, where $\mathbf{p}_i$ is the peculiar (i.e., thermal) momentum with respect to the streaming motion. The rate of change in position of a particle depends on the sum of its "thermal" fluctuation velocity and the streaming velocity at the position of the particle given by $\mathbf{u}(\mathbf{r}_i) = \mathbf{r}_i \cdot \nabla \mathbf{u}$. Equation (3) is the evolution of the peculiar momentum. The first term on the right-hand side denotes the sum $\mathbf{F}_i$ of the forces on particle i due to other particles. The second term couples the velocity field to the fluid and the last term couples the fluid to a heat bath, where ζ is a thermostat multiplier with inverse time units. These equations of motion result in a homogeneous fluid in which all the particles are subjected to the same external field (i.e., velocity gradient), and their dynamics is described by the same evolution equations.

By averaging the microscopic information over time and space, macroscopic quantities can be computed. For example, the pressure tensor,

$$\mathbf{P} = \frac{1}{V} \sum_{i=1}^{N} \left(\frac{\mathbf{p}_i \mathbf{p}_i}{m_i} + \frac{1}{2} \sum_{j \neq i} \mathbf{r}_{ij} \mathbf{F}_{ij} \right), \tag{4}$$

where $\mathbf{p}_i \mathbf{p}_i$ denotes the dyadic product of the peculiar momentum vectors, $\mathbf{r}_{ij} = \mathbf{r}_i - \mathbf{r}_j$, and $\mathbf{F}_{ij}$ is the interaction force acting on atom i due to atom j. Positive values of the diagonal components of the pressure tensor are associated with compression and negative values with tension. The pressure tensor is (besides the sign convention in some literature) identical to the stress tensor $\boldsymbol{\sigma}$ that is more common in rheology and the solid mechanics literature.[18,19]

The structure of this paper is as follows: The simulation details are presented in Sec. II. An introduction to the derivation of our proposed model is given in Sec. III. In Sec. IV, the simulation results are presented and used to calibrate and validate our model, and the presented model and results are discussed in Sec. V.

II. SIMULATION DETAILS

We simulate an atomic fluid whose interactions are mediated via the well-known Lennard-Jones (LJ) potential,[20] truncated at its minimum-energy distance $2^{1/6}\sigma$, where σ is the interaction length scale, and shifted up by the well-depth ϵ. This special version of the truncated and shifted LJ potential is known as the Weeks-Chandler-Andersen (WCA) potential[21]

$$U^{WCA}(r) = \begin{cases} 4\epsilon \left[\left(\frac{\sigma}{r}\right)^{12} - \left(\frac{\sigma}{r}\right)^{6} \right] + \epsilon, & r \leq 2^{1/6}\sigma, \\ 0, & r > 2^{1/6}\sigma. \end{cases} \tag{5}$$

All physical quantities presented are made dimensionless using the particle mass m and the LJ scales σ and ϵ, such that mass and the LJ scales become identical to unity in the simulations. The reduced quantities are length $\mathbf{r}_{ij} = \mathbf{r}^*_{ij}/\sigma$, number density $\rho = \rho^*\sigma^3/m$, temperature $T = \mathrm{k_B}T^*/\epsilon$, pressure tensor $\mathbf{P} = \mathbf{P}^*\sigma^3/\epsilon$, strain rate $\dot{\gamma} = \dot{\gamma}^*(m\sigma^2/\epsilon)^{1/2}$, time $t = t^*(m\sigma^2/\epsilon)^{-1/2}$, and viscosity $\eta = \eta^*\sigma^2(m\epsilon)^{-1/2}$. The equations of motion are integrated with a fourth-order Gear predictor-corrector algorithm with a time-step of $\Delta t = 0.001$ in reduced units.

We have performed NEMD simulations of a fluid containing $N = 512$ particles. The simulations are performed in the isokinetic-isochoric ensemble. The fluid density (i.e., the number of atoms and the system volume are fixed) and temperature are kept at a constant value, while the pressure tensor can depend on the state point and on the flow. The fluid density is $\rho = 0.8442$ and its temperature $T = 0.722$. The temperature is controlled using a Gaussian isokinetic thermostat.[22] This state point is near the triple point that a Lennard-Jones

fluid with the same parameters would have. This is the most extensively studied state point for MD simulations of a simple atomic fluid such as argon or krypton.[23] The simulations correspond to combinations of shear rates $\dot{\gamma} = 0,\ 0.1, \ldots, 0.5$ and elongational rates $\dot{\epsilon} = 0,\ 0.1, \ldots, 0.5$, such that the combinations of both deformations represent simple shear (5×), planar elongation (5×), and planar mixed flow (25×) simulations. Furthermore, additional shear flow simulations have been performed at shear rates $\dot{\gamma} = 0.025$, 0.05, and 0.15. The fluid is first equilibrated to reach a non-equilibrium steady state followed by a simulation of 500 units of time. The data are averaged over this steady-state time window and over ten equivalent simulations with different random initial configurations.

III. NEWTONIAN PRESSURE TENSOR

Equation (4) describes the pressure tensor for an atomic bulk fluid. The values in the resulting tensor are known to be related to the density and temperature of the fluid as well as to the velocity field. The relation between stresses and the fluid density and temperature can be described through an equation of state.[24,25] We concentrate more on finding a constitutive relation that describes how the pressure tensor depends on the velocity field. As detailed in Sec. II, we perform isochoric simulations, which correspond to traceless velocity gradients. Furthermore, we consider planar flows. Equation (1) satisfies these conditions, with at least one of $\dot{\gamma}$ and $\dot{\epsilon}$ non-zero. We start our derivation in this section by decomposing and rewriting the Newtonian pressure tensor, and we proceed with non-Newtonian pressure tensors in Sec. IV.

Any tensor can be decomposed into an isotropic part and a (traceless) deviatoric part. For an (idealized) incompressible Newtonian fluid, under an arbitrary flow type, we can write

$$\mathbf{P}_N = p_0 \mathbf{I} - \eta_0 \mathbf{S}, \tag{6}$$

such that the magnitude of the isotropic equilibrium part is determined by the hydrostatic pressure p_0 and the deviatoric viscous pressure tensor is given by the product of the strain rate tensor $\mathbf{S}$ and the zero-shear viscosity η_0.

The deviatoric pressure tensor can be rewritten in terms of a diagonal (principal) tensor rotated away from its principal orientation to the orientation of the pressure tensor.[26–28,56] We then obtain the product of a scalar to represent the magnitude of the deviatoric pressure tensor, and a matrix to denote its orientation. For a Newtonian fluid under any planar flow type with the velocity and its gradient in the x-y flow plane, Eq. (6) can be written as

$$\mathbf{P}_N = p_0 \mathbf{I} - \eta_0 s\, \mathbf{R}(\phi_S) \cdot \mathbf{I}_D \cdot \mathbf{R}^T(\phi_S), \tag{7}$$

$$\mathbf{I}_D \equiv \begin{pmatrix} 1 & 0 & 0 \\ 0 & -1 & 0 \\ 0 & 0 & 0 \end{pmatrix}, \tag{8}$$

$$\mathbf{R}(\phi) \equiv \begin{pmatrix} \cos\phi & -\sin\phi & 0 \\ \sin\phi & \cos\phi & 0 \\ 0 & 0 & 1 \end{pmatrix}, \tag{9}$$

where $s \equiv \sqrt{\frac{1}{2}\mathbf{S} : \mathbf{S}}$ is the magnitude of the strain rate tensor ($\mathbf{S} : \mathbf{S}$ is the second scalar invariant of $\mathbf{S}$), ϕ_S is the angle between the x-axis and the eigenvector that corresponds to the maximum eigenvalue of the strain rate tensor, $\mathbf{R}$ is a rotation matrix[29] that rotates around the z-axis (perpendicular to the flow plane) in counter-clockwise direction, and $\mathbf{I}_D$ is a (traceless) unit deviator matrix. The principal orientation angle of the strain rate tensor for a simple shear flow is $\phi_S = 45^\circ$ and for planar elongational flow it is $\phi_S = 0^\circ$. The orientation angle of the strain rate tensor for a planar mixed flow depends on the ratio between $\dot{\gamma}$ and $\dot{\epsilon}$ and is given by $\phi_S = \tan^{-1}(\dot{\gamma}/(2\dot{\epsilon}))/2$.

The product of the unit deviator and the scalar pre-factors denotes the principal deviatoric pressure tensor for a Newtonian fluid $\eta_0 s \mathbf{I}_D$. The diagonal elements of this term ($\eta_0 s$, $-\eta_0 s$, 0) are the eigenvalues of the deviatoric pressure tensor, while the rotation matrix $\mathbf{R}(\phi_S)$ consists of the corresponding eigenvectors. This notation replaces the usual expression in terms of shear stress and normal stresses by a notation that is not explicitly dependent on the Cartesian tensor orientation, but rather on tensor eigenvalues, eigen-system, and the velocity gradient magnitude.

The Newtonian pressure tensor assumes colinearity of the pressure tensor and strain rate tensor. This is often not the case for real fluids, such that $\phi_P \neq \phi_S$, where ϕ_P is the angle between the x-axis and the eigenvector that corresponds to the principal angle of the deviatoric pressure tensor. The difference between ϕ_P and ϕ_S is related to the viscoelasticity of the fluid and will be discussed in more detail in Sec. IV. An attempt to describe the pressure tensor of a viscoelastic fluid simply by replacing ϕ_S by ϕ_P in Eq. (7) is not enough to accurately describe the pressure tensor of a non-Newtonian fluid; a more sophisticated model is needed.

Equations (6) and (7) contain the equilibrium values of the shear-viscosity and hydrostatic pressure, whereas real fluids tend to exhibit shear thinning, pressure dilatancy, and normal stress differences when they are deformed sufficiently fast. Thus, this model, in which the viscous pressure (tensor) is a linear function of the shear rate, does not account for the more complex behavior, such as pressure dilatancy and normal stress differences, that some fluids exhibit even at small deformation rates. On the other hand, many existing models that do account for non-Newtonian phenomena are limited to only a specific type of flow. There is currently no simple model that quantifies the pressure tensor for a homogeneous non-Newtonian shear-thinning fluid subject to an arbitrary planar velocity gradient, while some less general relations have been developed for granular fluids under simple shear flow[30,31] or under radial deviatoric strain.[32]

IV. RESULTS AND DISCUSSION

A. Conventional description and an existing model

We first show simulation results in terms of shear stress and first normal stress difference, as is conventional. These quantities are relatively easy to extract from experiments, but are highly dependent on the type of flow. Figure 1 shows

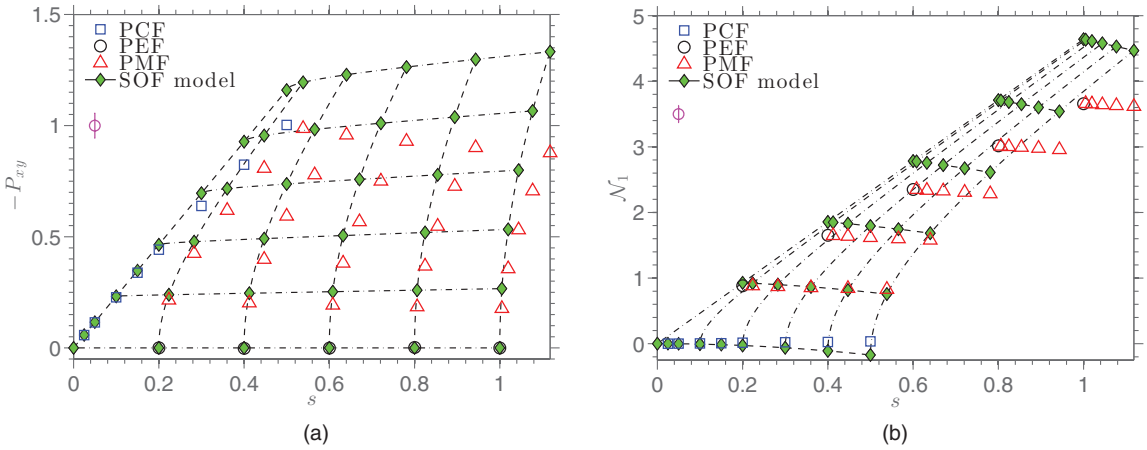

FIG. 1. NEMD simulation data of the shear stress (a) and first normal stress difference (b) for a fluid under shear (PCF), elongation (PEF), and planar mixed flow (PMF) compared to the prediction of the second-order fluid (SOF) model ($\rho = 0.8442$, $T = 0.722$).

the shear stress P_{xy} and the first normal stress difference $\mathcal{N}_1 = P_{yy} - P_{xx}$ of a WCA fluid plotted against the magnitude of the strain rate tensor $s \equiv \sqrt{\frac{1}{2}\mathbf{S} : \mathbf{S}} = \sqrt{\dot{\gamma}^2 + 4\dot{\epsilon}^2}$. The open markers denote the simulation results, whereas the filled markers correspond to a model prediction that is discussed below. Error bars are not shown since the standard errors are smaller than the plotted symbols. The average standard deviation of all data points is shown by the vertical bars directly below the legends. This is a measure for the fluctuations in the respective quantities. It is immediately clear that the values of the shown quantities strongly depend on the type of flow. For example, PCF, PEF, and PMF all show non-zero first normal stress differences, but no unified picture between the different flow types.

Nevertheless, the data for P_{xy} and $\mathcal{N}_1$ show trends with increasing $\dot{\gamma}$ and $\dot{\epsilon}$. The mixed flow data are in agreement with that reported by Hunt *et al.*[10] The data points on the x-axis of Figure 1(a) correspond to planar elongational flow simulations, whereas the data points close to the x-axis of Figure 1(b) correspond to shear flow simulations. A surprising observation is that the first normal stress difference increases with an increasing shear rate for PCF, while it decreases with an increasing shear rate $\dot{\gamma}$, at a constant elongational rate $\dot{\epsilon}$, for PMF. We have found from computer simulations at different state points (data not shown here) that the behavior of the first normal stress difference strongly depends on the state point of the fluid. Positive first normal stress differences are observed for very dense fluids, while the first normal stress differences become negative towards the semi-dilute regime, while the temperature is kept constant.

An existing family of models to describe the pressure tensor of non-Newtonian fluids makes use of a nonlinear tensorial approximation as a function of the flow field.[33–35] Second-order fluid (SOF) models are the simplest of such models that predict non-Newtonian phenomena, such as normal stress differences and shear dilatancy. These models can be employed to predict the pressure tensor of a fluid under any arbitrary flow field. For simple shear, planar elongation, or planar mixed flow, the second-order fluid prediction can be compared to NEMD simulation data. One, but by no means the only one, of these models will be briefly discussed here and a comparison is made between the prediction and simulation data for a simple WCA fluid under various planar flow types to assert that the use of a second-order model is not suitable to predict the pressure tensor of a shear-thinning fluid. In this model, equilibrium material constants are used to quantify the viscous part of the pressure tensor of a non-Newtonian fluid as a combination of elements that are linear and quadratic in terms of the deformation rate. Thus, not allowing for non-analytic behavior.

The pressure tensor in a second-order fluid can be described by the Rivlin-Ericksen constitutive relation,[36]

$$\mathbf{P} = p_0\mathbf{I} - \eta_0\mathbf{S} + \frac{\Psi_{1,0}}{2}\mathbf{A} - (\Psi_{1,0} + \Psi_{2,0})\mathbf{S}^2, \qquad (10)$$

$$\mathbf{A} \equiv \dot{\mathbf{S}} + \mathbf{S}\cdot\nabla\mathbf{u} + (\nabla\mathbf{u})^T\cdot\mathbf{S}, \qquad (11)$$

where $\Psi_{1,0}$ and $\Psi_{2,0}$ are the zero-shear rate first and second normal stress coefficients and $\mathbf{S}$ and $\mathbf{A}$ are the strain rate tensor and second Rivlin-Erickson tensor, respectively, where the second Rivlin-Erickson tensor is a function of the strain rate tensor and the velocity gradient. Furthermore, $\dot{\mathbf{S}} = \mathbf{0}$ in our case of steady flow denotes the derivative of $\mathbf{S}$ with respect to time.[37] This model is very simple, general, and based on the assumption that the non-equilibrium pressure tensor is analytic in terms of the deformation rate. The zero-shear rate first and second normal stress coefficients are defined as

$$\Psi_{\alpha,0} = \lim_{\dot{\gamma}\to 0}\Psi_\alpha(\dot{\gamma}), \qquad \alpha = 1, 2, \qquad (12)$$

where the non-equilibrium first and second normal stress coefficients, Ψ_1 and Ψ_2, are defined as

$$\Psi_1(\dot{\gamma}) = \frac{\mathcal{N}_1}{\dot{\gamma}^2} = \frac{P_{yy} - P_{xx}}{\dot{\gamma}^2}, \qquad (13)$$

$$\Psi_2(\dot{\gamma}) = \frac{\mathcal{N}_2}{\dot{\gamma}^2} = \frac{P_{zz} - P_{yy}}{\dot{\gamma}^2}. \qquad (14)$$

The first two terms on the right-hand side of Eq. (10) represent the Newtonian part (Eq. (6)), whereas the other two terms represent the deviation from Newtonian behavior. The

model predicts that the shear stress and first normal stress difference under a planar mixed flow are given by

$$P_{xy} = \dot{\gamma}(\eta_0 + \dot{\epsilon}\Psi_{1,0}), \tag{15}$$

$$\mathcal{N}_1 = \dot{\gamma}^2\Psi_{1,0} + 4\dot{\epsilon}\eta_0. \tag{16}$$

These expressions clearly show deviations from the Newtonian model when the shear rate is non-zero, $\dot{\gamma} > 0$. The predicted shear stress and first normal stress difference under planar elongational flow are identical to the Newtonian prediction. In the case of shear flow, the shear stress is simply Newtonian without shear thinning, while normal stress effects are accounted for. Combined stress effects arise for planar mixed flow.

Rather than evaluating the limit in Eq. (12), the zero-shear rate first normal stress coefficient can be calculated from time integrals over equilibrium correlation functions, as is described in detail by Hartkamp *et al.*[38] Using this method, the zero-shear rate first normal stress coefficient is calculated as $\Psi_{1,0} = 0.69 \pm 0.03$. The zero-shear rate shear viscosity is calculated as $\eta_0 = 2.32 \pm 0.01$ using the relevant Green-Kubo expression. The lines in Figure 1 indicate the trends predicted by the SOF model. The dashed lines correspond to constant $\dot{\epsilon}$, whereas the dashed-dotted lines correspond to constant $\dot{\gamma}$. The assumption of analytic behavior of the pressure tensor is known to be reasonably accurate at small deformation rates, but inaccurate for simple fluids at the state point and range of deformation rates that we study. As $\dot{\gamma}$ or $\dot{\epsilon}$ increases, so does the deviation from the SOF model prediction due to strain thinning. The inability of the model to predict the pressure tensor in the thinning regime makes an alternative approach desirable.

B. A new tensorial description

A symmetric pressure tensor contains six independent quantities, in general. This reduces to four independent quantities in the case of a steady-state planar flow, where the only non-zero shear stress is in the plane of flow. Therefore, the pressure tensor for a simple atomic fluid under a planar flow can be uniquely described with a model that contains a minimal four variables.

Rather than looking at the shear stress and first normal stress difference, we can look at quantities that are only dependent on the magnitude of the strain rate tensor and not on the type of flow. The thinning behavior that was seen in the shear stress and the normal stress differences in Figure 1 is related to the viscosity which is the proportionality constant between a driving force and the corresponding resulting flux.[13] An expression for the generalized viscosity can be derived from the steady rate of heat production per unit volume, as discussed by Hounkonnou *et al.*,[39]

$$\eta(\dot{\gamma}, \dot{\epsilon}) = -\frac{\mathbf{P}:\mathbf{S}}{\mathbf{S}:\mathbf{S}} = \frac{-\dot{\gamma}P_{xy} + \dot{\epsilon}\mathcal{N}_1}{\dot{\gamma}^2 + 4\dot{\epsilon}^2}. \tag{17}$$

The viscosity computed with this expression is independent of the choice of the coordinates in the flow plane, as the double tensor contractions in the numerator and denominator of the expression imply. When the elongational rate is zero, Eq. (17) simplifies to the well-known expression for shear viscosity $\eta = -P_{xy}/\dot{\gamma}$, whereas a situation in which the shear rate is zero results in the elongational viscosity $\eta = \mathcal{N}_1/(4\dot{\epsilon})$.

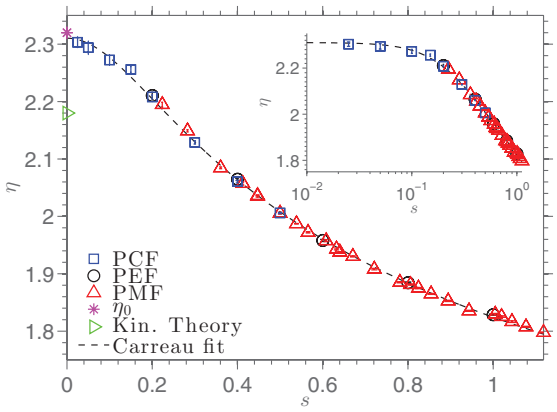

FIG. 2. Viscosity of a WCA fluid under shear (PCF), elongation (PEF), and mixed flow (PMF) at state point $\rho = 0.8442$, $T = 0.722$. The data are fitted with a Carreau model, and the equilibrium viscosity η_0 and a kinetic theory prediction are shown at $s = 0$. The inset contains the same data as a semi-log plot.

Figure 2 shows all our viscosity data of a WCA fluid under shear, elongation, and mixed flows as a function of s. The viscosity approaches the Newtonian viscosity η_0 in the equilibrium limit ($s \to 0$) and shows a monotonic decay with the strain rate magnitude. The fact that all data points in Figure 2 collapse onto a profile that is a function of the strain rate magnitude s only implies that the viscosity of the WCA fluid is independent of the flow type. It does, however, depend on the strength of the deformation rate, which is proportional to the square root of the rate of energy dissipation. The data are fitted with a Carreau function[40] as $\eta = \eta_0/(1 + c_{\eta 1}\, s^2)^{c_{\eta 2}}$, where $\eta_0 = 2.32 \pm 0.01$ is the zero-shear rate viscosity, $c_{\eta 1} = 21.21$, and $c_{\eta 2} = 0.076$. The positive power $c_{\eta 2}$ indicates that the fluid is shear thinning, whereas a negative number would correspond to a shear thickening fluid. Note that the Carreau equation is merely one of the fitting functions possible. Alternative examples include a simple power law[41] or the Cross model.[42] These are not shown here, since an extensive discussion of viscosity is not our main purpose. For comparisons of fitting functions, the reader is directed to Refs. 6 and 43–45. The zero-shear rate viscosity η_0 can be compared to a kinetic theory prediction for a dense fluid of rigid spheres.[46] We calculate an effective volume fraction $\nu = 0.4674$ by substituting our density, temperature, and zero-shear rate viscosity into Eq. (2) from Ref. 46. Using the effective volume fraction, temperature, and equilibrium pressure of the WCA fluid, the kinetic theory model predicts a zero-shear rate viscosity of $\eta^{KT} = 2.18$, which is 6.2% smaller than our simulation result.

1. Rotating the pressure tensor to its principal orientation

We start the derivation of our model by subtracting the first tensor invariant, i.e., the pressure $p = \mathrm{tr}(\mathbf{P})/3$, from the diagonal of the pressure tensor. What remains is the

(traceless) deviatoric pressure tensor $\mathbf{P}^D = \mathbf{P} - p\mathbf{I}$. The pressure is defined as the isotropic mean of the diagonal components of the pressure tensor; this is the first tensor invariant. The intermediate principal stress orientation of the deviatoric tensor, in a steady planar flow situation, is perpendicular to the plane of flow (while the major and minor principal stresses lie in the flow plane). This perpendicularity holds (as confirmed) within the statistical fluctuations of our data. The orientation of the deviatoric pressure tensor, which is equal to that of the full pressure tensor, is then given by a single angle ϕ_P between the x-axis and the eigenvector that corresponds to the largest eigenvalue of the deviatoric pressure tensor.

The Newtonian model in Eq. (7) expressed the pressure tensor as a function of s in terms of the principal orientation angle of the strain rate tensor ϕ_S and equilibrium material constants $\eta_0 = 2.32 \pm 0.01$ and $p_0 = 6.3903 \pm 0.0002$. Most fluids behave non-Newtonian when they are subjected to a sufficiently large deformation rate. The phenomenological transport coefficients and state variables can deviate from those predicted by linear response theory or measured from equilibrium molecular dynamics simulations. Consequently, the measured values of η and p for a fluid out of equilibrium can, and often do, deviate from the equilibrium values that are used in the Newtonian model and the SOF model. These deviations are due to shear thinning and pressure dilatancy, respectively. Colinearity between the pressure tensor and strain rate tensor may no longer be assumed for a viscoelastic fluid. Thus, for a non-Newtonian fluid, η, p, and ϕ_P can and will deviate from the equilibrium values that were used in the Newtonian model. Furthermore, an additional parameter may be required to uniquely describe the four independent non-zero components of the pressure tensor for a fluid in a planar flow situation. We first express the deviatoric pressure tensor in terms of its eigenvalues and its principal orientation (which is related to its eigenvectors), and then study the relation to the strain rate tensor.

The constitutive relation in Eq. (7) can be generalized for a non-Newtonian fluid. Doing so, we have to take into account that (1) the principal orientation of the deviatoric pressure tensor is not by definition identical to that of the strain rate tensor and (2) we do not know *a priori* the eigenvalues of the deviatoric pressure tensor, hence, we also cannot directly split the principal deviatoric pressure tensor in a scalar magnitude and a unit deviator matrix, as was done in Eq. (7). Without prior knowledge, we can write the pressure tensor for a fluid under planar flow as

$$\mathbf{P} = p\,\mathbf{I} + \mathbf{R}(\phi_P) \cdot \begin{pmatrix} -\lambda_1 - \lambda_2 & 0 & 0 \\ 0 & \lambda_1 & 0 \\ 0 & 0 & \lambda_2 \end{pmatrix} \cdot \mathbf{R}^T(\phi_P), \tag{18}$$

where $p = p_0 + \Delta p$ is the non-equilibrium pressure and the eigenvalues of the deviatoric pressure tensor are arranged as $\lambda_1 \geq \lambda_2 \geq \lambda_3 = -\lambda_1 - \lambda_2$. The order in subscripts is convention, while the order in magnitude of eigenvalues can be understood by thinking of planar elongational flow, in which the principal pressure tensor equals the pressure tensor, such that the diagonal elements of the deviatoric pressure tensor are equal to its eigenvalues. The stretch in the x-direction results in the smallest diagonal component of the pressure tensor, while the contraction in the y-direction corresponds to its largest diagonal component, and the out-of-flow-plane direction has an intermediate value.

In summary, the model expresses the pressure tensor in terms of non-equilibrium pressure p, the orientation angle of the principal deviatoric pressure tensor ϕ_P, and two independent eigenvalues of the deviatoric pressure tensor, λ_1 and λ_2. For further understanding, we study the dependence of these quantities on the velocity gradient.

2. Description of the non-Newtonian pressure tensor

Figure 3 shows the pressure and the eigenvalues of the deviatoric pressure tensor as functions of the magnitude of the strain rate tensor. Both graphs show clear trends with s and no visible dependency on the flow type. The pressure in Figure 3(a) increases with increasing s. This so-called pressure dilatancy is proportional to $\Delta p \propto s^{3/2}$ over almost two orders of magnitude, as shown in the inset. The error bars in the inset denote the standard deviation of the data points. This propor-

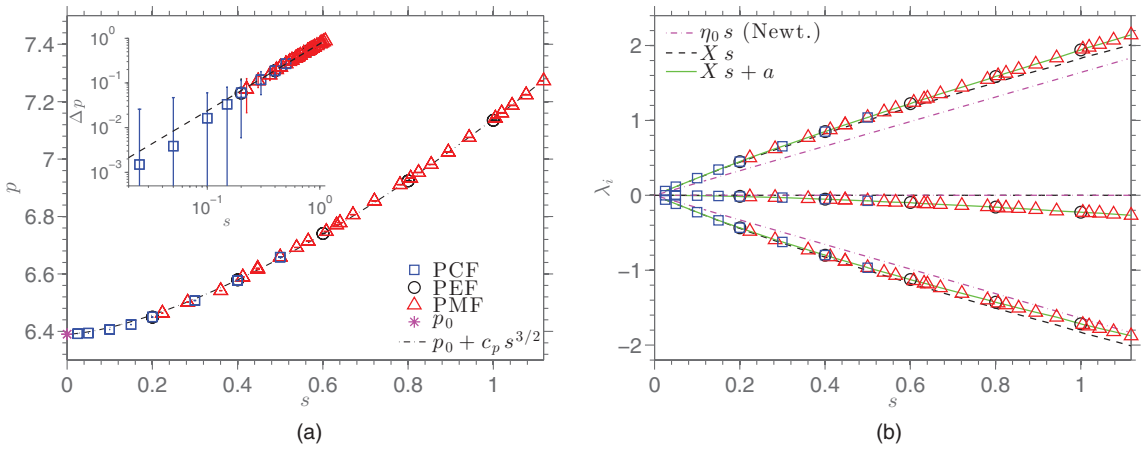

FIG. 3. Pressure (a) and eigenvalues of the deviatoric pressure tensor (b) as a function of the magnitude of the strain rate tensor ($\rho = 0.8442$, $T = 0.722$). The inset in (a) gives the proportionality between p and $s^{3/2}$ in a logarithmic graph, error bars give the standard error and the dashed line is the fit of the pressure dilatancy.

tionality has been reported in the literature for WCA fluids[47] as well as for a Lennard-Jones fluid at the same state point and comparable deformation rates,[48,49] and for a molten salt sheared at much higher rates.[45] Yet, the power law is based on a fit and is not based on theoretical arguments. The scaling with the deformation rate is different for very small s; a different proportionality $\Delta p \propto s^2$ has been reported for a WCA fluid near the LJ triple point, sheared at smaller rates $10^{-8} < \dot{\gamma} < 10^{-2}$, measured using the transient-time correlation function.[49] Our measurements at small deformation rates are not sufficient to confirm this different trend. The pressure in Figure 3(a) is fitted to a function of the form $p = p_0 + c_p s^{3/2}$, where p_0 is the equilibrium pressure and $c_p = 0.7492$. The eigenvalues of the deviatoric pressure tensor (Figure 3(b)) would be $(\lambda_1 = \eta_0 s, \lambda_2 = 0, \lambda_3 = -\lambda_1 - \lambda_2 = -\eta_0 s)$ for a Newtonian fluid. This prediction is shown in the figure with the dashed-dotted lines. To account for non-Newtonian phenomena in the plane of flow, an approximation can be made as $(Xs, 0, -Xs)$, where the middle eigenvalue corresponds to the direction perpendicular to the plane of flow and X is some variable that is determined later. Substituting Eq. (18) into Eq. (17) gives

$$\eta = \frac{2\lambda_1 + \lambda_2}{2s} \cos(2\Delta\phi), \tag{19}$$

where $\Delta\phi \equiv \phi_S - \phi_P$ represents the lagging of the pressure tensor relative to the strain rate tensor. The term $\cos(2\Delta\phi)$ is close to unity for all the data shown here, but this is not the case for example for a dilute fluid, where a longer relaxation time leads to a larger lagging angle.[57] Equation (19) is exactly valid for any steady planar flow. If we substitute the estimate $\lambda_1 = Xs$ and $\lambda_2 = 0$ into Eq. (19), we obtain

$$X = \frac{\eta}{\cos(2\Delta\phi)}. \tag{20}$$

This result is shown by the dashed lines in Figure 3(b). However, this approximation still assumes a zero intermediate eigenvalue, which is inconsistent with the simulation data. The data show that the magnitude of the intermediate eigenvalue is a function of s, but is independent of the flow type (i.e., the data for shear, elongation, and mixed flow all collapse on a single curve that is quantified later). An additional term can be added to the estimate of the eigenvalues as $(Xs + a, -2a, -Xs + a)$, where the value for a is calculated from the middle eigenvalue as $a = -\lambda_2/2$. Note that Eq. (19) remains exactly satisfied. The added correction term a is a measure for the out-of-flow-plane anisotropy of the pressure tensor. The new functional form for the eigenvalues leads to perfect agreement with the simulation data, as shown by the solid lines in the figure.[58]

Substituting the found functional form for the eigenvalues into Eq. (18) gives

$$\mathbf{P} = p\,\mathbf{I} + \mathbf{R}(\phi_P) \cdot \left(-\frac{\eta s}{\cos(2\Delta\phi)} \mathbf{I}_D + a \begin{pmatrix} 1 & 0 & 0 \\ 0 & 1 & 0 \\ 0 & 0 & -2 \end{pmatrix} \right) \cdot \mathbf{R}^T(\phi_P). \tag{21}$$

Since $\lambda_2 \neq 0$, the unit deviator matrix $\mathbf{I}_D$ is not sufficient for the description of the deviatoric pressure tensor and we have gained an additional tensorial term. This term is again written as the product of a scalar magnitude and a traceless matrix. The first term represents a planar, but non-colinear, deviatoric pressure tensor, while the second term quantifies the out-of-plane anisotropy. Both terms are traceless, and thus deviatoric, but the second is invariant under rotation in the plane of flow.

The tensor rotation on the right-hand side of Eq. (21) can be split into a rotation about an angle ϕ_S and an additional rotation by the (negative) lagging angle $-\Delta\phi = \phi_P - \phi_S$ to obtain the orientation of the pressure tensor ϕ_P. We know from Eqs. (6) and (7) that $\mathbf{S} = s\,\mathbf{R}(\phi_S) \cdot \mathbf{I}_D \cdot \mathbf{R}^T(\phi_S)$, such that the pressure tensor can be written as

$$\mathbf{P} = p\,\mathbf{I} - \frac{\eta}{\cos(2\Delta\phi)} \mathbf{R}(-\Delta\phi) \cdot \mathbf{S} \cdot \mathbf{R}^T(-\Delta\phi) + \sqrt{3}\,a\mathbf{I}_a, \tag{22}$$

$$\mathbf{I}_a \equiv \frac{1}{\sqrt{3}} \begin{pmatrix} 1 & 0 & 0 \\ 0 & 1 & 0 \\ 0 & 0 & -2 \end{pmatrix}, \tag{23}$$

where $\mathbf{I}_a$ is scaled such that the tensor has a scalar magnitude of 1, exactly like $\mathbf{I}_D$. This model contains the four state variables p, η, $\Delta\phi$, and a, which all are functions of the velocity gradient. The last term in the model is invariant under rotation around the z-axis and has equal contributions in the x and y directions.

It must be noted that the diagonal components of $\mathbf{I}_D$ and $\mathbf{I}_a$ are closely related to the in-plane η_- and out-of-plane η_* viscosity coefficients[50,51] that can be used as a measure of non-Newtonian behavior under shear flow. For simple shear flow, these coefficients are defined as $\eta_- \equiv \mathcal{N}_1/(2\dot{\gamma}) = (P_{yy} - P_{xx})/(2\dot{\gamma})$ and $\eta_* \equiv (P_{yy} - 2P_{zz} + P_{xx})/(4\dot{\gamma})$, where the occurrences of the normal pressure terms in the coefficients agree exactly with the diagonals of the planar and the non-planar terms in Eq. (21), respectively. The out-of-plane viscosity coefficient η_* is related to our out-of-plane anisotropy via $\eta_* = 6a/(4s)$. The data have confirmed that this relation is not limited to simple shear flow, but is valid for each of the planar flow types studied.

The parameter a in our model can be fitted against the magnitude of the strain rate tensor as $a = c_a s^{3/2}$ with $c_a = 0.1113$. The data for a and the corresponding fit are shown in Figure 4, where the fit slightly deviates from the data at small values of s. The inset indicates that the out-of-plane anisotropy a is almost perfectly proportional to the pressure dilatancy $p - p_0$, where the ratio between the out-of-plane viscous stresses and the pressure dilatancy $a/(p - p_0)$ approaches a constant value at large s. The ratio c_a/c_p is expected to be much smaller than unity for every planar flow. While the out-of-flow-plane anisotropy tends to zero for $s \to 0$, the ratio between a and $p - p_0$ diverges close to $s = 0$, since the denominator tends to zero faster than the numerator. The divergence turns out to be strongly related to the discrepancy at small s between the data for a and the fit of the data, and is

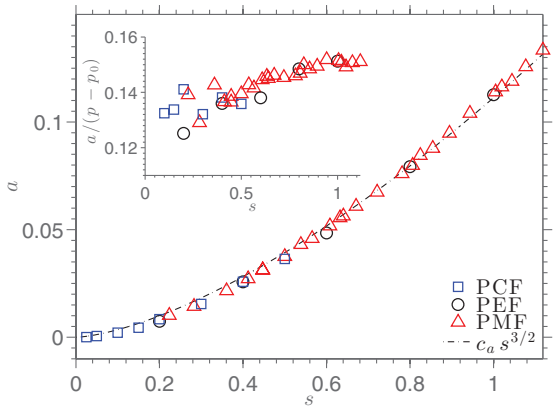

FIG. 4. The parameter a as a function of the magnitude of the strain rate tensor ($\rho = 0.8442$, $T = 0.722$). The inset shows the normalized anisotropy of the pressure tensor.

thus not considered to be physically meaningful. Alternative, better fits are not discussed here for the sake of brevity.

So far we have found that the parameters p, η, and a are independent of the flow type and only depend on the state point of the fluid and on s. We next study $\Delta\phi$. Figure 5 shows the orientation angles of the strain rate tensor ϕ_S, the pressure tensor ϕ_P, and the difference (lag) between both angles $\Delta\phi$ given in degrees. The lag angle is very small relative to the orientation angles, which makes it hard to measure with high accuracy. This difference is caused by distortion of the pair distribution function, which affects the configurational part of the pressure tensor, while the kinetic part of the pressure tensor remains isotropic. Note that the orientation of the distorted pair distribution function is by no means identical to that of the pressure tensor because the contribution that each interaction has to the pressure tensor depends not only on the relative position of the atoms but also on the absolute distance between them to determine the magnitude of the interaction force. Figure 5(b) shows that the lag angle divided by the magnitude of the vorticity $\omega = \dot{\gamma}/2$ collapses onto a single profile. Note that for small ω (and many of the data points with small values of s) the inaccuracy in the ratio $\Delta\phi/\omega$ becomes large. The profile is inversely proportional to $s + b$, where b is a constant that is inversely proportional to a time scale of the fluid in equilibrium, and thus related to the state point of the fluid. We can write the angle difference as $\Delta\phi = c_\phi\omega/(s + b)$ with fitting variables $c_\phi = 1.5883$ and $b = 0.1824$.

Evans *et al.*[52] suggested that the distortion of the microstructure of the fluid out of equilibrium should be proportional to a phenomenological relaxation time of the fluid. Similarly to the non-equilibrium structure of the fluid, also the viscoelastic lagging should be proportional to the relaxation time, such that we can write $\Delta\phi = c_\phi\,\omega/(s + b) = \tau\omega$ with $\tau \propto c_\phi/(s + b) = 1/(\alpha\tau_s^{-1} + \tau_0^{-1})$, where $\tau_0 = c_\phi/b$ and τ_s are competing equilibrium and non-equilibrium time scales and α is a proportionality constant. Different relaxation times can be defined and calculated. Many equilibrium and non-equilibrium relaxation times can be defined, for example, related to the transient response of the pressure tensor,[53] distortion of the pair distribution function,[54] or to the collision frequency.[55] For a fluid at equilibrium, for example, $\tau_1 \equiv \Psi_{1,0}/(2\eta_0) = 0.69/(2 \times 2.32) = 0.15$ was defined.[38]

3. Constitutive model for non-Newtonian fluid

In summary, the pressure tensor for a WCA fluid near the LJ triple point and under an arbitrary planar flow field in the thinning regime can be expressed in terms of four state variables:

$$\Delta p = c_p\, s^{3/2}, \tag{24}$$

$$\eta = \eta_0/(1 + c_{\eta 1}\, s^2)^{c_{\eta 2}}, \tag{25}$$

$$a = c_a\, s^{3/2}, \tag{26}$$

$$\Delta\phi = c_\phi\,\omega/(s + b), \tag{27}$$

where each quantity represents a deviation from Newtonian behavior, i.e., pressure dilatancy, strain thinning, out-of-plane pressure tensor anisotropy, and viscoelastic lagging. Substituting these parameters into Eq. (22) completes the presented

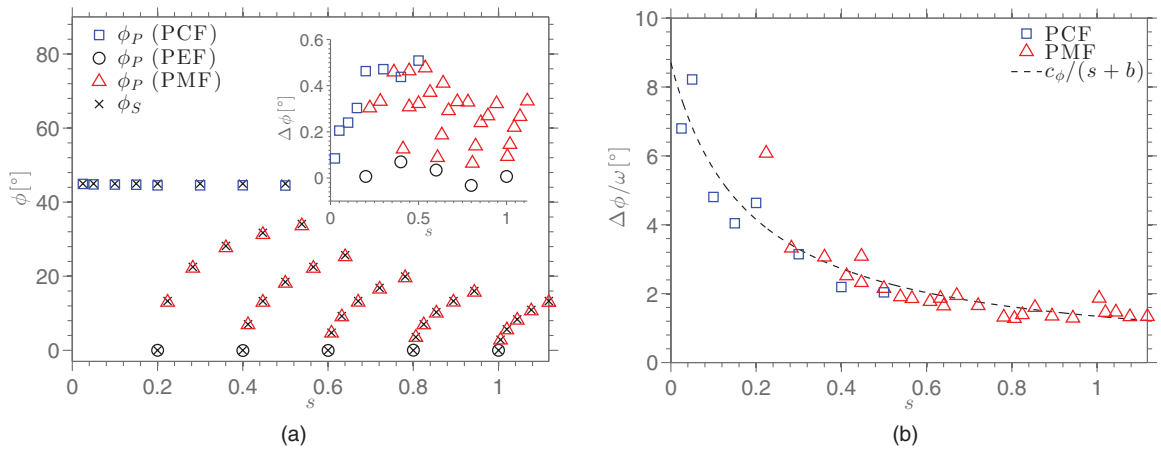

FIG. 5. Principal orientation angles (a) as a function of the magnitude of the strain rate tensor ($\rho = 0.8442$, $T = 0.722$), the inset shows the lag angle. In (b), the lag angle is scaled by the vorticity ω, such that the data collapse onto a single profile.

model. With the fitted parameters, the pressure tensor can be predicted for a WCA fluid near the LJ triple point for any given planar velocity gradient. The model contains a total of six fitting parameters (some of which can be interpreted as relaxation times) if the equilibrium fluid properties p_0 and η_0 are known. Alternatively, these also could be included as fitting parameters, which brings the total number to eight. The latter has been tried with our data as well (not shown). The fitted values for η_0 and p_0 were consistent, i.e., within the statistical uncertainty of our calculated values from equilibrium molecular dynamics (EMD) simulations.

In order to test the limits and predictive value of our model, we have performed simulations of a fluid under a larger deformation rate than that of the previous simulations. The model is tested for a fluid under a planar elongational flow with $\dot{\epsilon} = 1.0$, such that $s = 2$. The orientation angle of the pressure tensor should be zero for planar elongational flow, the simulation result gives $\phi_P = 0.0160$ with a larger relative uncertainty. The agreement between the model and the simulation results for pressure, viscosity, and anisotropy are -0.6%, -3.0%, and $+0.8\%$, respectively. This shows that the model predicts the pressure tensor with high accuracy even at larger deformation rates. We increase the deformation rate a little further and test the model for a fluid under planar mixed flow with $\dot{\gamma} = \dot{\epsilon} = 1.0$ corresponding to $s = \sqrt{5}$ and $\phi_S = 13.28^\circ$. The predicted values for p, η, a, and $\Delta\phi_P$ are all within 4% of the simulation results.

We have also performed simulations for $\dot{\gamma} = \dot{\epsilon} = 0.01$ ($s = \sqrt{5 \times 10^{-4}}$) to verify the convergence towards Newtonian behavior near equilibrium. We have measured $\eta = 2.33 \pm 0.02$ and $p = 6.3897 \pm 0.0004$, which means that both quantities agree within the standard error with the values calculated with EMD simulations. Deviations from the Newtonian limiting behavior are too small to be measured accurately from NEMD simulations very close to equilibrium unless significantly more statistics is accumulated, or alternative techniques are used to enhance it.[11]

V. SUMMARY AND CONCLUSIONS

We have presented a framework to predict the pressure tensor for a fluid under arbitrary steady homogeneous planar flows. The framework describes the full pressure tensor in terms of four variables, which is the minimum number of variables required. The variables involve a quantitative description of non-Newtonian phenomena being strain-rate thinning viscosity, pressure dilatancy, viscoelastic lagging, and out-of-plane pressure tensor anisotropy.

Steady-state non-equilibrium molecular dynamics simulations have been performed for a WCA fluid near the LJ triple point. Simulations for shear flow, planar elongational flow, and combined shear and elongation show the same deviations from Newtonian behavior. All of these results, when expressed in terms of functions of the driving field strength s, the vorticity ω, and the equilibrium fluid properties collapse onto master curves. This shows that the pressure tensor can be predicted for each planar flow, making it possible to predict the full pressure tensor for a simple fluid under various types of planar flows without having to produce these flows explicitly in a simulation or experiment. Prior knowledge is required about the equilibrium properties and the non-equilibrium scaling of the fluid at the state point of interest. This can be easily obtained from one series of simple shear flow simulations, only varying s.

We have found that the principal pressure tensor for a simple atomic fluid is solely dependent on the scalar magnitude of the flow field at the chosen state point of the fluid. This was shown in Figure 3. The Cartesian pressure tensor is also dependent on the shear rate, the vorticity, and the principal orientation of the strain rate tensor. However, the orientation of the pressure tensor is defined relative to the orientation of the strain rate tensor, not explicitly dependent on the Cartesian coordinate system.

The non-Newtonian fluid model is calibrated with results from various simulations over a wide range of deformation rates. Furthermore, the model was used to predict (extrapolate) the pressure tensor for simulations much further away from equilibrium and very close to equilibrium. The predictions were very accurate for all model variables up to large deformation rates.

The model is valid for the spatially homogeneous systems used here, but the same framework should be equally beneficial for the study of shear-banding or confined fluids if the model is proven to be locally valid too. Inhomogeneity creates a complicated problem, since the state point of the fluid and thus also the flow properties become functions of position. The possibility of applying a similar framework to a confined fluid problem has been investigated in Ref. 27. It can also straightforwardly be applied, for example, to polymeric fluids, colloidal systems, ionic liquids, or granular fluids,[28] where insight in non-Newtonian behavior would be of great benefit. Especially in polymeric rheology, many complicated empirical models exist that require many more parameters and do not explicitly quantify the deviations from Newtonian behavior in a compact formulation and for arbitrary planar velocity gradients as presented here. Our model could simplify the description of molecular rheology dramatically, although modifications of the model would be required to appreciate the various mechanisms that are responsible for the deviations from Newtonian behavior. For example, the lagging angle of a molecular fluid would be highly affected by the orientation and stretching of molecules, and thus related to the size and internal structure of molecules.

All data presented in this work correspond to a single density and temperature. The functional forms of all of the non-Newtonian quantities have been validated at five different state points (data not shown here). It was found that the (fitting) parameters depend strongly on the state point of the fluid. An extensive study at various state points could provide more insight in the dependence of the non-Newtonian rheology on density and temperature. This study is currently being undertaken.

A possible next step towards a "complete" description of the non-Newtonian pressure tensor should be an extension of the model to allow for transient or time-dependent flows. This would require an extensive study of relaxation dynamics to non-equilibrium steady states and to equilibrium after cessation of steady flow. Preliminary studies at a range of

deformation rates and flow types show consistent relaxation behavior in the linear response regime, but distinctive differences when the response is a non-linear function of the deformation rate (i.e., in the shear thinning regime). The range of deformation rates considered in this study is far into the non-linear regime, where transient behavior is extremely complicated. In order to attempt an extension towards a time-dependent description of the pressure tensor, a study with lower deformation rates is advised.

[1]A. M. Kraynik and D. A. Reinelt, Int. J. Multiphase Flow **18**, 1045 (1992).
[2]B. D. Todd and P. J. Daivis, Phys. Rev. Lett. **81**, 1118 (1998).
[3]D. J. Evans and G. P. Morriss, Phys. Rev. A **30**, 1528 (1984).
[4]D. J. Evans and G. P. Morriss, Phys. Rev. Lett. **51**, 1776 (1983).
[5]T. A. Hunt and B. D. Todd, J. Chem. Phys. **131**, 054904 (2009).
[6]N. Galamba, C. A. Nieto de Castro, and J. F. Ely, J. Chem. Phys. **122**, 224501 (2005).
[7]B. D. Todd, Phys. Rev. E **58**, 4587 (1998).
[8]M. W. Evans and D. M. Heyes, Mol. Phys. **69**, 241 (1990).
[9]D. M. Heyes, Chem. Phys. **98**, 15 (1985).
[10]T. A. Hunt, S. Bernardi, and B. D. Todd, J. Chem. Phys. **133**, 154116 (2010).
[11]R. Hartkamp, S. Bernardi, and B. D. Todd, J. Chem. Phys. **136**, 064105 (2012).
[12]A. J. C. Ladd, Mol. Phys. **53**, 459 (1984).
[13]D. J. Evans and G. P. Morriss, *Statistical Mechanics of Nonequilibrium Liquids*, 2nd ed. (Cambridge University Press, Cambridge, 2008).
[14]P. J. Daivis and B. D. Todd, J. Chem. Phys. **124**, 194103 (2006).
[15]B. D. Todd and P. J. Daivis, Mol. Simul. **33**, 189 (2007).
[16]W. G. Hoover, D. J. Evans, R. B. Hickman, A. J. C. Ladd, W. T. Ashurst, and B. Moran, Phys. Rev. A **22**, 1690 (1980).
[17]W. Hoover, C. G. Hoover, and J. Petravic, Phys. Rev. E **78**, 046701 (2008).
[18]J. M. Dealy, J. Rheol. **28**, 181 (1984).
[19]L. Malvern, *Introduction to the Mechanics of a Continuous Medium* (Prentice Hall, Englewood Cliffs, New Jersey, 1969).
[20]J. E. Jones, Proc. R. Soc. London, Ser. A **106**, 463 (1924).
[21]J. D. Weeks, D. Chandler, and H. C. Andersen, J. Chem. Phys. **54**, 5237 (1971).
[22]D. J. Evans, W. G. Hoover, B. H. Failor, B. Moran, and A. J. C. Ladd, Phys. Rev. A **28**, 1016 (1983).
[23]M. F. Pas and B. J. Zwolinski, Mol. Phys. **73**, 471 (1991).
[24]D. A. Kofke, J. Chem. Phys. **98**, 4149 (1993).
[25]L. V. Woodcock, AIChE J. **52**, 438 (2006).
[26]M. Alam and S. Luding, Phys. Fluids **15**, 2298 (2003).
[27]R. Hartkamp, A. Ghosh, T. Weinhart, and S. Luding, J. Chem. Phys. **137**, 044711 (2012).
[28]T. Weinhart, R. Hartkamp, A. R. Thornton, and S. Luding, "Coarse-grained local and objective continuum description of 3D granular flows down an inclined surface," Phys. Fluids (to be published).
[29]P. K. Kundu, I. M. Cohen, and D. R. Dowling, *Fluid Mechanics*, 5th ed. (Elsevier Science, Amsterdam, 2011).
[30]C. Thornton and L. Zhang, Philos. Mag. **86**, 3425 (2006).
[31]J. Sun and S. Sundaresan, J. Fluid Mech. **682**, 590 (2011).
[32]C. Thornton and L. Zhang, Geotechnique **60**, 333 (2010).
[33]H. Markovitz and B. D. Coleman, Phys. Fluids **7**, 833 (1964).
[34]B. D. Coleman and W. Noll, Arch. Ration. Mech. Anal. **6**, 355 (1960).
[35]P. J. Daivis, M. L. Matin, and B. D. Todd, J. Non-Newtonian Fluid Mech. **147**, 35 (2007).
[36]G. A. Nunez, G. S. Ribeiro, M. S. Arney, J. Feng, and D. D. Joseph, J. Rheol. **38**, 1251 (1994).
[37]M. Slemrod, Arch. Ration. Mech. Anal. **146**, 73 (1999).
[38]R. Hartkamp, P. J. Daivis, and B. D. Todd, Phys. Rev. E **87**, 032155 (2013).
[39]M. N. Hounkonnou, C. Pierleoni, and J. P. Ryckaert, J. Chem. Phys. **97**, 9335 (1992).
[40]H. Bruus, *Theoretical Microfluidics*, Oxford Master Series in Condensed Matter Physics (Oxford University Press, USA, 2007).
[41]B. D. Todd, Phys. Rev. E **72**, 041204 (2005).
[42]M. M. Cross, J. Colloid Sci. **20**, 417 (1965).
[43]P. Prathiraja, P. J. Daivis, and I. K. Snook, J. Mol. Liq. **154**, 6 (2010).
[44]R. F. Berg, J. Rheol. **48**, 1365 (2004).
[45]J. Delhommelle and J. Petravic, J. Chem. Phys. **118**, 2783 (2003).
[46]J. Jenkins, Granular Matter **10**, 47 (2007).
[47]K. P. Travis, D. J. Searles, and D. J. Evans, Mol. Phys. **95**, 195 (1998).
[48]J. Ge, G. Marcelli, B. D. Todd, and R. J. Sadus, Phys. Rev. E **64**, 021201 (2001).
[49]D. J. Evans and G. P. Morriss, Phys. Rev. A **36**, 4119 (1987).
[50]S. Hess, Physica A **118**, 79 (1983).
[51]S. Hess and H. J. M. Hanley, Int. J. Thermophys. **4**, 97 (1983).
[52]D. J. Evans, H. J. M. Hanley, and S. Hess, Phys. Today **37**, 26 (1984).
[53]R. C. Picu and J. H. Weiner, J. Chem. Phys. **107**, 7214 (1997).
[54]H. J. M. Hanley, J. C. Rainwater, and S. Hess, Phys. Rev. A **36**, 1795 (1987).
[55]S. Luding, Pramana **64**, 893 (2005).
[56]R. Hartkamp, Ph.D. dissertation, University of Twente, 2013.
[57]This has been confirmed with simulations at different state points;[56] data not shown here.
[58]The predictive quality of Eqs. (25)–(27), as represented by the green solid lines, is within 0.5 % of the simulation data.